Acta Cryst A FOUNDATIONS ADVANCES
ISSN 2053-2733

Topological crystallography of gas hydrates

Sergey V. Gudkovskikh[a] and Mikhail V. Kirov[a,b]*

[a]Institute of the Earth Cryosphere SB RAS, Tyumen, 625000, Russian Federation, and [b]Tyumen State Oil and Gas University, Tyumen, 625000, Russian Federation. *Correspondence e-mail: mkirov@ngs.ru

Received 22 January 2015
Accepted 6 May 2015

Edited by W. F. Kuhs, Georg-August University Göttingen, Germany

Keywords: topological crystallography; quotient graph; clathrate hydrates; proton disorder.

A new approach to the investigation of the proton-disordered structure of clathrate hydrates is presented. This approach is based on topological crystallography. The quotient graphs were built for the unit cells of the cubic structure I and the hexagonal structure H. This is a very convenient way to represent the topology of a hydrogen-bonding network under periodic boundary conditions. The exact proton configuration statistics for the unit cells of structure I and structure H were obtained using the quotient graphs. In addition, the statistical analysis of the proton transfer along hydrogen-bonded chains was carried out.

1. Introduction

Crystallography is a well established science. However, it is impossible to describe the structure of ordinary ice and other ice-like systems using the standard methods of crystallography. The main reason is that the ice itself is not a crystal in the usual sense of the word (Petrenko & Whitworth, 1999; Malenkov, 2009). The crystal lattice of ice and ice-like systems determines only the position of the oxygen atoms. The positions of the hydrogen atoms are disordered. The number of defect-free proton configurations is huge and increases exponentially with the size of the system (Bernal & Fowler, 1933; Pauling, 1935). At the same time, these configurations may differ significantly in the binding energy and other characteristics (Kuo & Singer, 2003; Hirsch & Ojamäe, 2004; Yoo *et al.*, 2009; Takeuchi *et al.*, 2013). Furthermore, in ice and ice-like systems the positions of protons are constantly changing due to random migration of protons along hydrogen-bonded chains (Petrenko & Whitworth, 1999). Therefore, in a real experiment, we have to deal with a superposition of many states. The theoretical description of the structure of ice-like systems should take into account the variety and diversity of proton configurations, as well as the dynamic variability of the structure of the proton subsystem. In this situation, representative sets of the proton configurations may be interesting. The sets of all proton configurations for the unit cells or extended cells with periodic boundary conditions are of most interest (Hirsch & Ojamäe, 2004; Kirov, 2010; Takeuchi *et al.*, 2013). They can be used for computer simulation.

Periodic boundary conditions (PBCs) for ice-like systems imply that the orientations of water molecules must be coordinated not only inside the modelling box, but also on the opposite boundaries of this box. Generation and enumeration of such correlated structures is not a trivial problem of combinatorial optimization. Methods for solving these problems are well known. However, there is an alternative approach, which allows us to circumvent the problem of boundary correspondence. This approach is based on topo-

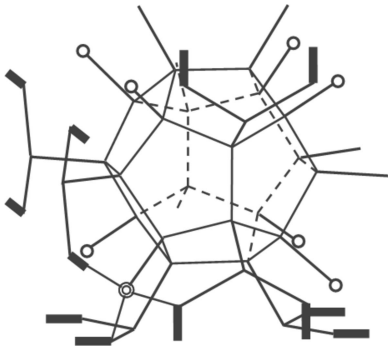

logical crystallography (Sunada, 2012). The origin of this scientific discipline is connected with the name of A. F. Wells (1977). One of the most important concepts of topological crystallography is a quotient graph of crystal structure (Chung *et al.*, 1984; Delgado-Friedrichs & O'Keeffe, 2005; Eon, 2005; Blatov & Proserpio, 2011). It is also called a finite fundamental graph or factor graph. According to Krivovichev (2013), the quotient graph of an infinite 3-periodic network is the finite graph that is obtained by projection of all translationally equivalent vertices (edges) of the network onto one vertex (edge) of the finite graph.

For an ice-like system, the quotient graph is a compact 4-connected graph. This graph depicts adequately the topology of the hydrogen bonding both inside the modelling box and at the interface with adjacent boxes. This graph has no outer unrealized hydrogen bonds. Hydrogen bonds, which pass through the opposite sides of the modelling box, are short-circuited due to PBCs. As a result, we obtain a finite uniform digraph which completely depicts the hydrogen-bonding topology and proton disorder combinatorics of the initial crystal lattice under PBCs. Configurations of the initial unit cell with PBCs and configurations of the quotient graph are in one-to-one correspondence. Any of them can be easily restored by the other. But it is more convenient to deal with a finite graph. For example, it is much easier to study the statistical regularities of the proton transfer in hydrogen bonds because the quotient graph has no boundaries. Note also the fact that topological crystallography definitely has a heuristic potential for finding new hydrogen-bonding topologies. So, using this approach for the unit cell of ice Ih, we predicted a new form of ice bilayer (Kirov, 2012).

In this article we present the quotient graphs for the unit cells of well known clathrate hydrate structures I and H (see, for instance, Sloan, 1998). Using these graphs, the statistics of proton disorder in the unit cells under PBCs were studied. It allows us to confirm our previous results for the total number of proton configurations (Kirov, 2010). This is especially important as there are some differences between our results and the results of Takeuchi *et al.* (2013). On the basis of topological crystallography, we have obtained a quasi-one-dimensional representation of the unit cells of structures I with PBCs in two perpendicular directions. It allows us to confirm our previous result for the unit cell ($1 \times 1 \times 1$) and to calculate the exact number of Bernal–Fowler configurations for the extended cell ($2 \times 1 \times 1$). Also we have studied the statistics of random proton transfer along hydrogen-bonded chains in structures I and H, using the quotient graphs.

2. Topological closure and the quotient graphs

2.1. Hexagonal ice Ih

Before proceeding to clathrate hydrates, let us consider the structure of the orthorhombic unit cell of hexagonal ice consisting of eight water molecules (Fig. 1*a*). The small size of the unit cell allows us to consider this cell as a toy-model to demonstrate the basic concepts of topological crystallography, as applied to ice-like systems. We indicate by arrows the direction of the hydrogen bonds: from the proton donor to the acceptor. Because of PBCs in the vertical direction, the hydrogen bonds indicated in Fig. 1(*a*) by arrows have the same direction. From topological and combinatorial standpoints, we can consider that corresponding upper and lower water molecules are connected directly. The fact is that in the topological sense the crystal as a whole becomes equivalent to hexagonal bilayer ice. Further application of PBCs in the remaining two directions (Fig. 1*b*) leads to the structures shown in Figs. 1(*c*), 1(*d*). Each of these quasi-one-dimensional structures represents an extended unit cell of ice Ih with PBCs in transverse directions (Kirov, 2012). In both cases, application of PBCs along the two-section fragments leads to the structure which is equivalent to the initial unit cell of ice Ih with PBCs in all three directions. The resulting structure (Fig. 1*e*) is the same for both quasi-one-dimensional systems (Figs. 1*c*, 1*d*). This is just the quotient graph of ice Ih with PBCs on the faces of the orthorhombic

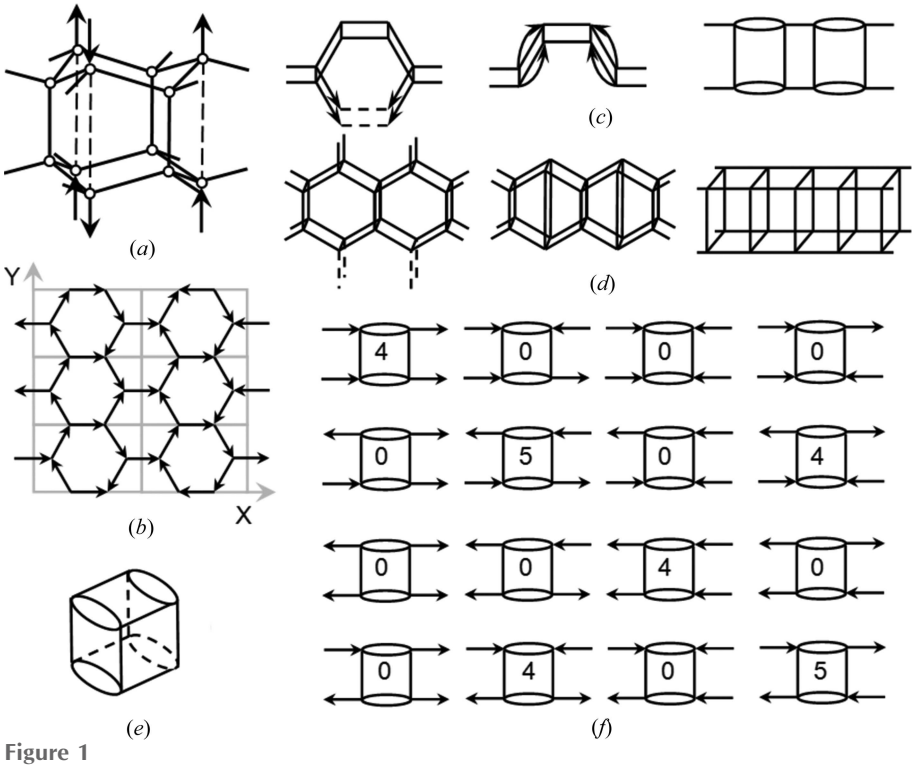

Figure 1
Topological transformations of hexagonal ice fragments: (*a*) the structure of hexagonal ice Ih; (*b*) view from above, the unit cells are shown by grey lines; (*c*), (*d*) two-layer ice fragments; (*e*) quotient graph for orthogonal unit cell of hexagonal ice Ih; (*f*) calculation schema for the transfer matrix.

unit cell. An appearance of artificial biangle cycles is due to the small size of the cell used.

Topological transformations of this kind facilitate calculation of the total number of defect-free configurations that satisfy the well known ice rules (Bernal & Fowler, 1933). They are also known as Bernal–Fowler rules. These rules imply that two arrows are incoming and two are outgoing at each vertex. The total number of configurations in any quasi-one-dimensional system can be found using the transfer matrix method (Kramers & Wannier, 1941). Recently, such calculations were carried out for ice-like systems (Kirov, 2009, 2013; Tokmachev & Dronskowski, 2010, 2011). The numbers of Bernal–Fowler configurations in a separate section for all possible directions of the external horizontal hydrogen bonds on the left and right are shown in Fig. 1(*f*). They form the transfer matrix **M**, the size of which is determined by the total number of possible directions of the external bonds from one side of the section. Using the transfer matrix method, the number of proton configurations of an *n*-element ice-like system with PBCs can be calculated from the following well known formula:

$$X_n = \mathrm{Tr}(\mathbf{M}^n) = \sum_{i=1}^{N} \lambda_i^n. \qquad (1)$$

As mentioned, the unit cell of ice Ih corresponds to two elements of the strip. The number of Bernal–Fowler configurations in this cell is equal to the trace of the square of the transfer matrix: $\mathrm{Tr}(\mathbf{M}^2)$. To put it another way, taking into account that the eigenvalues of the 4×4 transfer matrix (see Fig. 1*f*) can be easily calculated and the values are $\lambda_1 = 9$, $\lambda_{2,3} = 4$, $\lambda_4 = 1$ (Kirov, 2012), the total number of configurations in the unit cell of ice Ih is $9^2 + 2\times4^2 + 1 = 114$. This number is well known (Lekner, 1998), but the approach, which is based on topological crystallography, allows us to find it easily.

2.2. Structure I clathrate hydrate with periodicity in two directions

The unit cell of structure I contains 46 water molecules (Fig. 2*a*) which enclose two different types of cavities: a pentagonal dodecahedral cavity D (5^{12}) and a tetracaidecahedral cavity T ($5^{12}6^2$). Two large cavities T can be easily seen in Fig. 2(*a*). The unit cell includes 36 molecules of the two depicted cavities T (only positions of oxygen atoms are shown). In addition, ten side molecules (six at the left and four at the rear face) can be related to this unit cell. These molecules are depicted by black circles. As a result, we have all 46 molecules per one unit cell.

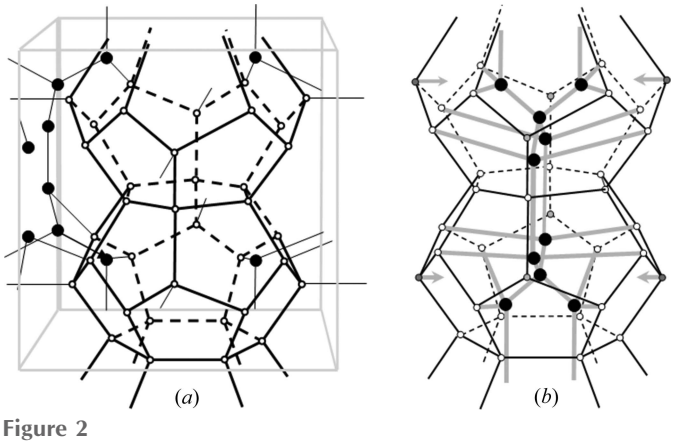

Figure 2
Topological transformations of the unit cell for structure I of clathrate hydrates.

There are two molecules on each of the four vertical edges of the cubic cell. We can make a conclusion, taking into account the symmetry: in an equivalent compact graph the four pairs correspond to one pair of vertices. The pair is located on a vertical line that passes through the centre of the unit cell. Besides, because of the symmetry, two remaining pairs of molecules of the left lateral face (and their images to the right) are mapped on the parallel plane that passes through the centre of the cell. This forms a hexagon (Fig. 2*b*) which is perpendicular to the plane of the figure. Analogously, four water molecules arranged on the rear face and their images (on the front face) are projected on the parallel plane, passing through the centre of the cell. As a result, inside the vertical row of cavities T, a chain of hexagons is formed. Conservation of the hydrogen-bonding topology leads to the graph shown in Fig. 2(*b*). It should be added that four opposite pairs of vertices (small grey circles) are directly connected to each other (two pairs are shown by arrows).

In a topological sense, the structure obtained is absolutely equivalent to the initial unit cell (Fig. 2). In order to calculate the total number of Bernal–Fowler configurations, we can use the transfer matrix method (see §2.1). Note that, in this case, two sections of a quasi-one-dimensional system (two cavities T) are included in one unit cell. The size of the transfer matrix is equal to the number of all different directions of outer hydrogen bonds for each section. Note that only allowed configurations of the hexagonal cycles might be used. The number of Bernal–Fowler configurations for a hexagonal ring of water molecules is $3^6 + 1 = 730$ (Kirov, 2009). But here it is necessary to take into account four cases of the direction of two vertical hydrogen bonds which pass through horizontal hexagonal rings. Therefore, the size of the transfer matrix is 2920×2920. Another important point is that here we need two different transfer matrices, as the cavities are differently oriented. The first matrix **A** specifies the number of allowed configurations A_{ij} in the lower cavity for all possible directions of defining hydrogen bonds at the bottom and top of the cavity (hexagon and two vertical hydrogen bonds). The second matrix **B** specifies the number of proton configurations in the upper cavity B_{jk} for all directions of outer hydrogen bonds. For the whole unit cell, the transfer matrix **M** is a product of two matrices: **A** and **B**. When PBCs also apply in the vertical direction then, according to equation (1), the number of proton configurations $X_n = \mathrm{Tr}\,(\mathbf{M}^n)$, where $\mathbf{M} = \mathbf{A} \cdot \mathbf{B}$, and n is the length of the extended unit cell ($1 \times 1 \times n$). The transfer matrices **A** and **B** were calculated using a special program. It was found that for the unit cell with PBCs in all three directions the number of Bernal–Fowler configurations $X_1 = \mathrm{Tr}\,(\mathbf{M}) = 822\,823\,440$. Along the way, we have obtained the exact number of proton configurations in the extended cell ($1 \times 1 \times 2$): $X_2 = \mathrm{Tr}\,(\mathbf{M}^2) = 208\,662\,423\,394\,711\,512$. The number X_1 is

consistent with our previous result (Kirov, 2010), which was obtained using a more cumbersome method. At the same time, this number is significantly different from the number obtained by Takeuchi *et al.* (2013), which is equal to 685 686 200, *i.e.* exactly 5/6 of our result.

Note that the transfer matrix **M** allows us to calculate the exact asymptotic value of the residual entropy for infinite extension of the unit cell in one direction ($1 \times 1 \times n$), *i.e.* when $n \rightarrow \infty$. According to equation (1), the asymptotic number of proton configurations is determined by the maximum eigenvalue of the transfer matrix. The maximum eigenvalue was calculated using the iterative power method (Larson, 2013): $\lambda_{max} \simeq 3.6012886 \times 10^8$. Therefore, the asymptotic value of the residual entropy for the one-dimensionally extended unit cell of structure I is $S = \ln(\lambda_{max})/46 \simeq 0.428304$. This is a limit of the sequence $S_1 = \ln(X_1)/46 = 0.446266$, $S_2 = \ln(X_2)/92 = 0.433472$ *etc*. Because of cubic symmetry of the unit cell for structure I, all variants of the one-dimensional expansion ($n \times 1 \times 1$, $1 \times n \times 1$ and $1 \times 1 \times n$) are equivalent.

2.3. The quotient graphs of the unit cells of sI and sH clathrate hydrates

For the unit cell of structure I with three-dimensional PBCs, the direction of the upper and lower hydrogen bonds in Fig. 2(*b*) should be identical. So we may consider them as the same hydrogen bonds that connect corresponding nodes of the hydrogen-bond network. The resulting completely closed network is one of the representations of the quotient graphs for initial crystal lattices. There are many drawings of the same quotient graph. Topologically, they all are completely equivalent to the initial structures with PBCs. It is convenient to depict all nodes in the interior of one cavity and on its surface. The new choice of the unit cell for the structure I which corresponds to lateral shift by half a period is shown in Fig. 3 (*cf.* Fig. 2*a*). Besides 20 molecules of small cavity D there are eight inner molecules, which are indicated by white circles. For one of them (double circle) the topology of hydrogen bonding may be seen in Fig. 3. In addition, six molecules are located on each face of the cubic unit cell. Overall, there are 20 + 8 + 36/2 = 46 molecules per unit cell. Pairs of translationally equivalent hydrogen bonds on the surface are shown by bold lines. For the cavity-based quotient graphs it is possible to use a simple algorithm to compute the coordinates of all vertices of the quotient graph:

(i) Specify and fix the coordinates of all vertices for one cavity.

(ii) Enumerate all vertices and list all inner hydrogen bonds that do not belong to the cavity surface, *i.e.* for each inner hydrogen bond specify the pairs of vertices taking into account PBCs.

(iii) For all listed hydrogen bonds that do not belong to the cavity, write the sum of the squares of the lengths, as a function of free (unknown) coordinates.

(iv) Minimize this function in order to find the coordinates of inner vertices of the cavity.

Note that minimizing the sum of squares of lengths of all inner hydrogen bonds (all partial derivatives are zero) is equivalent to a system of linear equations. At the same time, the standard software may be used to find the minimum of a function of several variables without calculating derivatives. In addition, the vertices obtained in this way can be easily redistributed in radial directions by using elementary transformations. They might be concentrated toward the centre or,

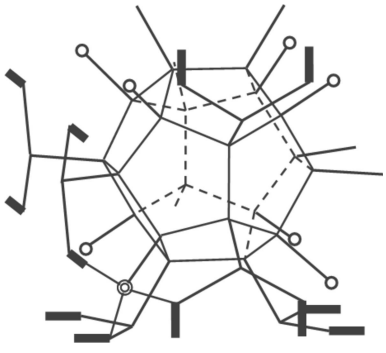

Figure 3
Positions of oxygen atoms of water molecules and hydrogen bonding in the unit cell of structure I.

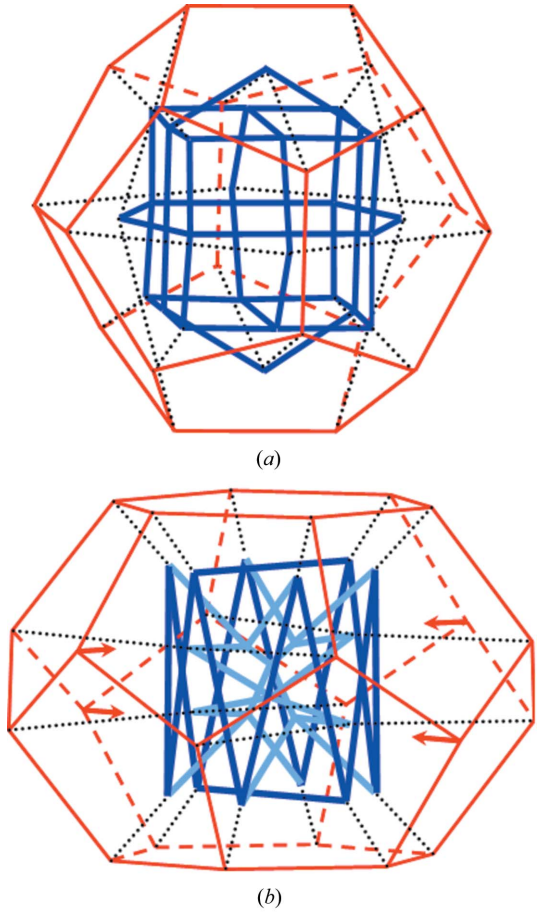

Figure 4
Quotient graphs of structure I which are based on the cages D (*a*) and T (*b*).

on the contrary, away from the centre. A similar method has been used previously to construct planar images (Schlegel diagrams) for large multicage hydrate structures (Kirov, 2003).

For the quotient graph of structure I, the hydrogen-bonding topology (pairs of vertices for each hydrogen bond) can be specified using Fig. 2(*a*), Fig. 2(*b*) or Fig. 3. The quotient graph based on cavity D is shown in Fig. 4(*a*). The inner part of the graph is a cube (eight molecules), belted by three hexagons (18 molecules). Taking into account 20 molecules of external cavity D, we have all 46 molecules of the unit cell. Molecules that belong to both the cube and hexagons take part in the formation of four internal hydrogen bonds. Each molecule in the cube vertex, along with three internal hydrogen bonds, forms one bond with the outer cavity. Finally, molecules of hexagons which do not belong to the cube are connected with two molecules of the external cavity.

The usability, *i.e.* clarity and understandability, of the quotient graphs strongly depends on the location of inner vertices. The cubic arrangement of internal vertices in the quotient graph (Fig. 4*a*) was obtained using the above algorithm and additional redistribution of internal points in the radial direction. Note that the cubic symmetry of the unit cell of structure I is in good agreement with the symmetry of the external cavity. The second representation of the quotient graph that is based on cavity T is less convenient (Fig. 4*b*). Finding the best visual representation of the quotient graph is a separate problem. But it is important to stress that here we have two different drawings of the same quotient graph. They both correspond to the same unit cell with PBCs. Therefore, it is sufficient to have at least one easy-to-use quotient graph.

The hexagonal structure H is shown in Fig. 5(*a*). This structure has three types of cavities. There are two small cavities D (5^{12}) and one small cavity D′ ($4^3 5^6 6^3$) per unit cell. Both of these cavities are composed of 20 molecules. In addition, there is a large cavity E ($5^{12}6^8$) that consists of 36 molecules (Sloan, 1998). The location of large and small cavities can be seen in Fig. 5(*a*). In general, there are 34 water molecules per unit cell. Therefore, it is difficult to construct a quotient graph using the large cavity E. The positions of all molecules in the unit cell are depicted in Fig. 5(*b*). However, the hexagonal symmetry of the unit cell (see equivalent hydrogen bonds in Fig. 5*b*) makes the quotient graphs, which are based on cavities D and D′, less obvious (Fig. 6). Here, at the beginning, we have used the algorithm that was described above. Further, using some topology-preserving transformations, we have tried to make the inner part of the graphs clearer, as much as possible.

The quotient graphs (Figs. 4, 6) greatly simplify the problem of enumeration of all Bernal–Fowler configurations. Recall that, in such configurations, at each vertex two arrows are incoming and two arrows are outgoing. The simplest algorithm for enumerating all hydrogen-bond directions includes a large number of nested loops: 92 for structure I and 68 for structure

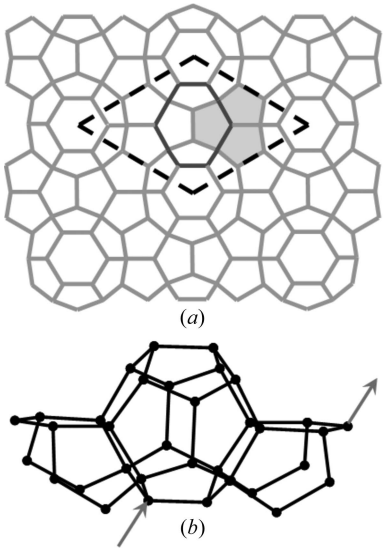

Figure 5
(*a*) Hexagonal structure H, containing cavities D (at the centre of the unit cell which is shown by a dashed line), D′ (grey colour) and E (around the unit cell). (*b*) Position of oxygen atoms in the unit cell of structure H. Two equivalent hydrogen bonds are shown by grey arrows.

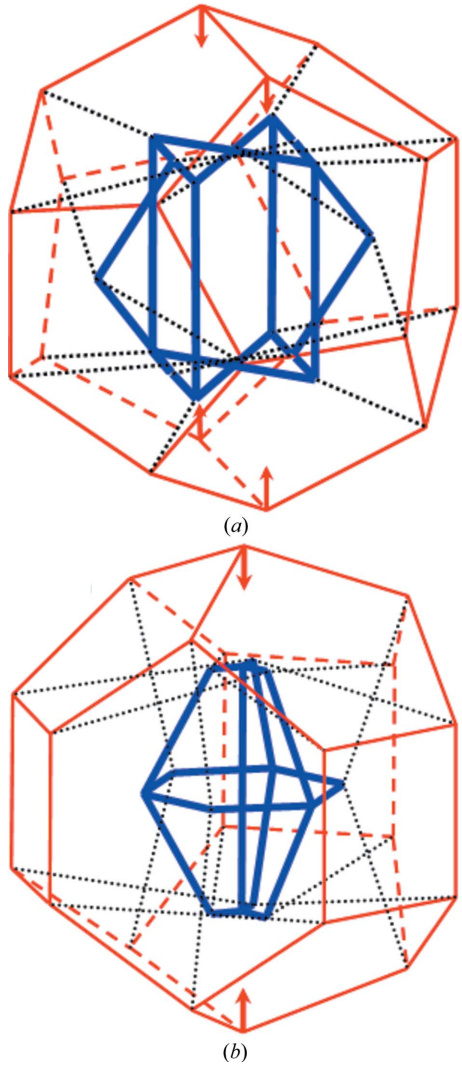

Figure 6
Quotient graphs of structure sH which are based on the cages D (*a*) and D′ (*b*).

H, because the number of hydrogen bonds is twice the number of molecules. For each proton configuration, it is necessary to verify the Bernal–Fowler rules at each vertex of the quotient graph. Note that it is technically impossible to sort out all combinations of hydrogen-bond directions, since the numbers of variants for structures I and H are 2^{92} or 2^{68}, respectively. However, when the verification of the Bernal–Fowler rules is located not within all the loops, but is distributed between the loops, depending on the maximum number of hydrogen bonds incident to a given node, the algorithm becomes quite acceptable. For structures I and H, the computing times are about 1 h and 1 min, respectively, for a usual PC. These times are dependent on the method of hydrogen-bond numbering. For the quotient graphs of structures I and H, the total number of configurations are equal to 822 823 440 and 5 568 720 in complete agreement with our previous result (Kirov, 2010), as well as with the result of §2.2.

3. The statistics of proton transfer along hydrogen-bonded chains

As noted in §1, the structure of the proton subsystem of ice and clathrate hydrates is very changeable. The quotient graphs of clathrate structures can be useful to study the topological regularities of the proton transfer along hydrogen-bonded chains. The advantage of the quotient graphs over ordinary crystallographic depiction is that closed hydrogen-bonded cycles within the unit cell and on its faces are completely equivalent. Therefore, we do not have the dependence on the choice of the unit cell (although the image of the quotient graph has a certain arbitrariness). For example, in the above algorithm, different cavities may be used as an outer shell. But this choice does not disturb the cyclic structure of the graph and the topology of hydrogen bonding as a whole.

Changing the structure of the proton subsystem in the ice and gas hydrate frameworks is due to the appearance of structural defects, that violate the Bernal–Fowler rules. The defects cause random shifts of protons along unidirectional hydrogen-bonded chains (Petrenko & Whitworth, 1999). In the model representation, the proton motion produces a reversal of the arrows along the random directed path. The closing of the circuit causes the disappearance of the defect. For the quotient graphs, the distributions in the length of the n-step paths (number of hydrogen bonds) are shown in Fig. 7.

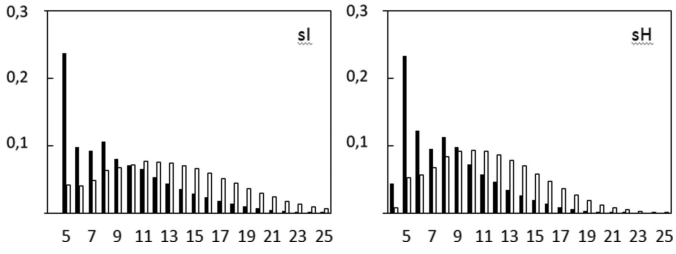

Figure 7
The probability of occurrence (fraction) of n-membered unidirectional hydrogen-bonded chains in the quotient graph: closed loops (black bars) and paths which are ended by the self-crossing (white bars).

White bars correspond to the paths which are ended by the self-crossing. Black bars correspond to the closed loop only. In both cases, 10 000 000 chains were used to construct the probability distribution. Note that some of these cycles correspond to artificial infinite loops passing through the unit cell (see seven-member cycles in structure I). All these artificial cycles can be excluded as we have initial coordinates of oxygen atoms. However, it is remarkable that a large part of all the closed circuits in Fig. 7 are pentagonal. Even a greater fraction of the elementary (hexagonal) cycles was obtained for large simulation boxes of hexagonal and cubic ice (Rahman, 1972). However, it does not mean that in bulk ice and gas hydrates the structural change occurs so frequently due to the reversal of the direction of hydrogen bonds inside the elementary cycles (pentagons, hexagons). The point is that when the cyclic closure was found, we changed the direction of hydrogen bonds only within the revealed closed loops, and we ignored the initial portion of the chain together with the point of the defect. For a more realistic simulation of the structural changes, it is necessary to take into account the initial part of the circuit, as well as the interaction between the defects.

4. Concluding remarks

The structural features of ice-like systems, which are due to the presence of a huge number of nonequivalent proton configurations, justify the emergence of new theoretical approaches. A detailed investigation of the properties of clathrate hydrates can be performed on the basis of a representative set of symmetrically distinct proton configurations. In particular, complete lists of all Bernal–Fowler configurations for different sizes of the cells are interesting as the representative sets. A construction of the quotient graphs for clathrate frameworks is a new way of visualizing the hydrogen-bonded network, which facilitates the study of the proton disorder. For systems with PBCs, this approach best corresponds to the adjacency matrix, in which cycles at the surface of, and inside, the cell are also equivalent. For larger unit cells, such as the unit cell of structure II, containing 136 molecules, (Sloan, 1998) or for expanded unit cells, the visual perception of the quotient graphs is rather difficult. In this situation, the understandable and comfortable quotient graphs for structures I and H are also of methodological interest for development and debugging of general algorithms for the study of the structure and properties of clathrate hydrates, taking into account the proton disorder.

Structures I and H have symmetry $Pm\bar{3}n$ and P6/mmm. The orders of the crystal classes (number of non-translated symmetry operations), according to Hahn (2006), are 48 and 24, respectively. For each of these unit cells, we can approximately estimate the number of symmetrically distinct proton configurations by dividing the total numbers of configurations 822 823 440 and 5 568 720 by the orders of the crystal classes, because the vast majority of the proton configurations in these rather large cells are not symmetrical (symmetry $P1$). The exact numbers of the symmetry-distinct proton configurations in these cells are equal to 17 151 190 and 232 261, respectively

(Kirov, 2010). The approximation error is less than 0.1% in both cases. Note that the quotient graphs may well be used to analyse the symmetry of proton configurations. For this it is necessary to specify the permutations of the serial numbers of bonds and nodes, corresponding to the generators of symmetry groups, and then calculate the permutation corresponding to the rest of the symmetry operations. These permutations can be used in the selection of symmetry-distinct proton configurations. Similarly, we can analyse the generalized symmetry (anti-symmetry), which is related to the reversal of all hydrogen bonds (Kirov, 2014). For large cells it allows us to reduce the list of different configurations approximately twice. Finally, note that for each configuration of the oriented quotient graph we can estimate the total dipole moment of the unit cell as a vector sum of hydrogen-bond dipoles. These vectors are determined in the initial geometry and directed from one oxygen to another. Each configuration of the quotient graph determines only the signs of these directions (+ or −).

Acknowledgements

We would like to thank Elena Kirova for assistance in the preparation of the manuscript. The reported study was partially supported by RFBR, research project No. 15-03-04274 and by the Interdisciplinary Integration Project SB RAS No. 144.

References

Bernal, J. D. & Fowler, R. H. (1933). *J. Chem. Phys.* **1**, 515–548.
Blatov, V. A. & Proserpio, D. M. (2011). *Modern Methods of Crystal Structure Prediction*, edited by A. R. Oganov, pp. 1–28. Weinheim: Wiley–VCH.
Chung, S. J., Hahn, Th. & Klee, W. E. (1984). *Acta Cryst.* A**40**, 42–50.
Delgado-Friedrichs, O. & O'Keeffe, M. (2005). *J. Solid State Chem.* **178**, 2480–2485.
Eon, J.-G. (2005). *Acta Cryst.* A**61**, 501–511.
Hahn, Th. (2006). Editor. *International Tables for Crystallography*, Vol. A, *Space-group Symmetry*, 1st online ed. Chester: International Union of Crystallography.
Hirsch, T. K. & Ojamäe, L. (2004). *J. Phys. Chem. B*, **108**, 15856–15864.
Kirov, M. V. (2003). *J. Struct. Chem.* **44**, 420–428.
Kirov, M. V. (2009). *Phys. A Stat. Mech. Appl.* **388**, 1431–1445.
Kirov, M. V. (2010). *Crystallogr. Rep.* **55**, 353–361.
Kirov, M. V. (2012). *J. Stat. Phys.* **149**, 865–877.
Kirov, M. V. (2013). *Phys. A Stat. Mech. Appl.* **392**, 680–688.
Kirov, M. V. (2014). *J. Phys. Chem. B*, **118**, 13341–13348.
Kramers, H. A. & Wannier, G. H. (1941). *Phys. Rev.* **60**, 252–262.
Krivovichev, S. V. (2013). *Mineral. Mag.* **75**, 2687–2702.
Kuo, J.-L. & Singer, S. J. (2003). *Phys. Rev. E Stat. Nonlin. Soft Matter Phys.* **67**, 016114.
Larson, R. (2013). *Elementary Linear Algebra*, 7th ed. Boston, MA: Brooks/Cole.
Lekner, J. (1998). *Phys. B Condens. Matter*, **252**, 149–159.
Malenkov, G. (2009). *J. Phys. Condens. Matter*, **21**, 283101.
Pauling, L. J. (1935). *J. Am. Chem. Soc.* **57**, 2680–2684.
Petrenko, V. F. & Whitworth, R. W. (1999). *Physics of Ice.* Oxford University Press.
Rahman, A. (1972). *J. Chem. Phys.* **57**, 4009–4017.
Sloan, E. D. Jr (1998). *Clathrate Hydrates of Natural Gases*, 2nd ed. New York: Marcel Dekker, Inc.
Sunada, T. (2012). *Jpn. J. Math.* **7**, 1–39.
Takeuchi, F., Hiratsuka, M., Ohmura, R., Alavi, S., Sum, A. K. & Yasuoka, K. (2013). *J. Chem. Phys.* **138**, 124504.
Tokmachev, A. M. & Dronskowski, R. (2010). *J. Phys. A Math. Theor.* **43**, 325001.
Tokmachev, A. M. & Dronskowski, R. (2011). *J. Comput. Chem.* **32**, 99–105.
Wells, A. F. (1977). *Three-Dimensional Nets and Polyhedra*. New York: Interscience.
Yoo, S., Kirov, M. V. & Xantheas, S. S. (2009). *J. Am. Chem. Soc.* **131**, 7564–7566.